This is a pre-print of an article published in Journal of Electronic Materials, 2018, Volume 47, Issue 9, pp 5077–5082.
The final authenticated version is available online at: https://doi.org/10.1007/s11664-018-6381-8

Photoluminescence Imaging and LBIC Characterization of Defects in mc-Si Solar Cells

L.A. Sánchez[1,2], A. Moretón[1], M. Guada[1], S. Rodríguez-Conde[1], O. Martínez[1], M.A. González[1] and J. Jiménez[1],

1.—GdS-Optronlab, Dpto. Física de la Materia Condensada, Universidad de Valladolid, Edificio LUCIA, Paseo de Belén 19, 47011 Valladolid, Spain. 2.—e-mail: lasandom92@gmail.com

ABSTRACT

Nowadays the photovoltaic market is dominated by multicrystalline silicon (mc-Si) based solar cells with around 70% of worldwide production. In order to improve the quality of the Si material, a proper characterization of the electrical activity in mc-Si solar cells is essential. A full-wafer characterization technique like photoluminescence imaging (PLi) provides a fast inspection of the wafer defects at the expense of the spatial resolution. On the other hand, a study of the defects at a microscopic scale can be achieved through the light-beam induced current (LBIC) technique. The combination of these macroscopic and microscopic resolution techniques allows a detailed study of the electrical activity of defects in mc-Si solar cells. In this work, upgrade metallurgical-grade (UMG) Si solar cells are studied using these two techniques.

KEY WORDS: solar cells, multicrystalline silicon, UMG silicon, LBIC, photoluminescence

INTRODUCTION

Multicrystalline silicon (mc-Si) is currently the basis of the photovoltaic (PV) market due to its low production cost and relatively high efficiency. Upgraded metallurgical-grade silicon (UMG Si) has raised as an alternative to the traditional purification obtained by Siemens process because of the reduced production cost and time [1, 2]. Although the Siemens process produces the purest material, solar cells fabricated with wafers from UMG Si have achieved efficiencies around 20% [3].

UMG Si contains more impurities, like shallow acceptors and donors, which reduce the carrier diffusion lengths and limit the cell efficiency [4]. In order to improve the quality of the UMG Si, it is essential to know the type of defects and the detrimental role played by the trapping centers for the photogenerated carriers. Photoluminescence imaging (PLi) and light-beam induced current (LBIC) techniques have demonstrated to be powerful characterization tools for measuring the electrical activity of defects in mc-Si solar cells [5-8]. In PLi, the surface of the sample is excited with optical radiation to emit luminescence and a CCD camera is used to acquire the luminescence emission signal. This technique does not require electrical contacts and is applicable not only to solar cells, but also to bricks, as-cut wafers and processed wafers [9]. PLi provides a macroscopic spatially-resolved image of the electrical activity of a solar cell in a short time (seconds), depending on the quantum efficiency of the camera. Silicon CCD cameras can detect only a very small portion of the Si band to band luminescence emission, usually it requires long exposure times. However, InGaAs cameras are sensitive to the luminescence spectrum of Si, and operate at shorter exposure times than the Si CCD cameras. Dark contrasted areas in the images obtained by PLi can be associated with grain boundaries, dislocations, micro-cracks, etc. In LBIC, a laser beam is focused and scanned point by point over a surface area of the solar cell, and the generated electron-hole pairs produce a photocurrent [10]. This photocurrent is collected at each point of the selected area and its intensity is governed by the trapping of minority carriers. LBIC images reveal the spatial distribution of the trapping centers. This technique, instead of PLi, allows a very high spatial resolution, but it is time consuming as compared to PLi. In this work we study defects in UMG mc-Si solar cells at macroscopic and microscopic scales using these two techniques.

EXPERIMENTAL

PL imaging was measured by the homemade setup represented schematically in Fig. 1a. The PLi excitation system contains four 20 W laser diodes (808 nm wavelength). The photoluminescence emission of the solar

cell is captured in a dark environment with a 1392x1040 pixels Si-CCD camera (PCO 1300 solar). In order to get a full image of the solar cell a 12.5 mm focal length objective is coupled to the camera. A longpass filter with a cutoff wavelength of 900 nm was mounted in front of the camera to remove the background light. PL emission was also captured with an InGaAs camera (Hamamatsu C12741-03).

A homemade LBIC system was used to obtain higher detailed information about the defects in the solar cells. The scheme of the LBIC setup is shown in Fig. 1b. The LBIC apparatus consists of four excitations wavelengths from two dual laser diodes (Omicron). The laser lines are 639, 830, 853 and 975 nm, and they allow to achieve different penetrations depths. In the studies presented here only the 853 nm line was used. A beam-splitter divides the output beam of the laser (10 mW) into two beams. One of them is used to measure variations in the output power through a photodiode. The other one is directed into a trinocular microscope which focuses the laser onto the solar cell. Different objectives (20x, 50x, 100x) enable studies up to a very high spatial resolution, circa 1 μm for the 100x objective. A Si-CCD camera coupled to the top ocular is used to collect the light reflected by the sample and drive the auto-focus system through edge detection. The LBIC scanning is obtained by moving the sample in an *x-y-z* motorized translation stage (Prior Scientific) over areas as large as 76.7 x 114.5 mm^2 and step sizes as small as 1 μm. The photocurrent generated is collected by an electrometer (Keithley Instruments) and data acquisition and hardware control was developed in LabVIEW.

UMG mc-Si solar cells provided by Silicio Ferrosolar were characterized through the PLi and LBIC techniques. The measures were carried out on three series of UMG mc-Si solar cells. A-series have efficiencies ranging between 17.4 and 17.6%, B-series have efficiencies between 16.8 and 17.0% and C-series have efficiencies between 16.4 and 16.8%.

RESULTS AND DISCUSSION

Figs. 2a—c show the PL images obtained in three solar cells corresponding respectively to series A, B and C. These images presented dark areas that mainly correspond to grain boundaries and intragrain defects. A first look to these images shows that the C-series solar cell image contains a greater number of dark areas. The three series of measured solar cells yielded different values of photoluminescence intensity signal. Higher values of efficiency produced higher values of the intensity of the PL emission of the solar cell. This PL intensity signal is expressed through the mean value of the intensity over all the pixels of the PLi image. An almost linear dependence is shown in Fig. 2d, where the maximum, minimum and mean value

of this PL intensity signal is plotted for each solar cell series. Very similar results were found with the two cameras used in the experiment, the Si CCD camera and the InGaAs camera. In the second one, the exposure times used are lower because of the higher quantum efficiency of the InGaAs sensor around the wavelength at which silicon emits. In particular, the exposure time values used in the experiments are 150 ms for the InGaAs camera against 30 seconds for the Silicon CCD.

Fig. 3 shows the PL image of a C-series solar cell as well as the LBIC map of a highly defective zone obtained with a 20x objective. Whereas the PLi measurement showed an almost uniform dark zone because of the poor spatial resolution, the LBIC map allowed to appreciate the structure of the defects, which appears as an array of dark contrasted lines, thanks to the greater spatial resolution obtained with this technique. The LBIC contrast is higher due to the large photocurrent generated by the laser beam over a small area. The LBIC measure took about 24 hours to map this 18000x18000 μm^2 region of the solar cell with a lateral resolution of 60 µm. More detailed information about these defects can be obtained by using a high magnification objective. Figs. 4a—c show 400x400 μm^2 LBIC maps of A, B and C-series solar cells using a 100x objective. These measurements revealed a slightly bright contrasted line along the core of the defects in all the series. This local bright contrast is probably due to a depletion of impurities. The impurities tend to accumulate at both sides of this bright line resulting in dark regions of high trapping activity. Fig. 4d shows the normalized photocurrent profiles across the lines marked in Fig. 4a—c. The ratio between currents generated in non-defective and defective areas is essentially the same on the three solar cells, so the lower efficiencies in B and C series can be explained not as an increase of the electrical activity of the defects but as the consequence of a greater density of defects.

Some of the B and C-series solar cells presented micrometric size dark spots around the defects in some regions (Fig. 5a), with a pronounced drop in the photocurrent. Fig. 5b shows the reflected light map of a C-series sample obtained with the Si-CCD camera coupled to the microscope. This map revealed information about the higher photocurrent generated at the core of the defects as a consequence of a lower reflectivity, but no information is obtained about these dark spots. UMG Si contains more metallic impurities than traditional solar grade Si, so these dark spots can be explained as an accumulation of metallic impurities which give rise to clusters with high electrical activity [11]. The reflected map also showed low reflective regions without high capture rates around them in the corresponding LBIC measurement. The goal of future studies will be an accurate measurement of the total light power reflected by the cell in order to provide a

tool to calculate the internal quantum efficiency (*IQE*) and effective diffusion length (L_{eff}) of the minority carriers, using the different excitation wavelengths integrated in the LBIC system.

CONCLUSION

In this work, we studied the electrical activity of defects in several UMG mc-Si solar cells of known efficiencies through PLi and LBIC techniques. PLi allowed a fast full-wafer observation of the cells, with a good correlation between the mean value of PL intensity signal and the solar cell efficiencies. A detailed description of the defective areas revealed by PLi was achieved by high spatial resolution LBIC mapping. The photocurrent ratio between non-defective and defective areas was the same for the three series of cells. Solar cells with lower efficiencies presented dark spots around some of the defects. Reflected light mapping allowed to establish a correlation between LBIC maps and surface features but no information about these dark spots was revealed.

ACKNOWLEDGEMENTS

This work was supported by the Spanish MINECO project, ref. ENE2014-56069-C4-4-R and "Junta de Castilla y León (Spain)" project number VA081U16. We thank Silicio Ferrosolar for providing the samples studied in this work.

REFERENCES

[1] N. Yuge, M. Abe, K. Hanazawa, H. Baba, N. Nakamura, Y. Kato, Y. Sakaguchi, S. Hiwasa and F. Aratani, Prog. Photovolt: Res. Appl. 9, 203–209 (2001).

[2] D. Kohler, B. Raabe, S. Braun, S. Seren and G. Hahn, in *Proceedings of the 24th European Photovoltaic Solar Energy Conference* (2009), pp. 1758–1761.

[3] F. Rougieux, C. Samundsett, K. C. Fong, A. Fell, P. Zheng, D. Macdonald, J. Degoulange, R. Einhaus, and M. Forster, Prog. Photovolt: Res. Appl. 24, 725–734 (2016).

[4] M. Forster, P. Wagner, J. Degoulange, R. Einhaus, G. Galbiati, F. Rougieux, A. Cuevas and E. Fourmond, Sol. Energy Mater Sol. Cells 120, 390–395 (2014).

[5] T. Trupke, B. Mitchell, J. W. Weber, W. McMillan, R. A. Bardos and R. Kroeze, Energy Procedia 15, 135-146 (2012).

[6] M. Bliss, X. Wu, K. Bedrich, T. Betts and R. Gottschalg, IET Ren. Pow. Gener. 9, 446–452 (2014).

[7] B. Moralejo, M. A. González, J. Jiménez, V. Parra, O. Martínez, J. Gutiérrez and O. Charro, J. Electron. Mater. 39, 663–670 (2010).

[8] M.K. Juhl, M.D. Abbot, T. Trupke, IEEE J. Photovolt. 7, no. 4, 1074–1080 (2017).

[9] B. Moralejo, A. Tejero, O. Martínez, M. A. González, J. Jiménez and V. Parra, in *Proceedings of the 2013 Spanish Conference on Electron Devices* (2013), pp. 353–356.

[10] B. Moralejo, V. Hortelano, M. A. González, O. Martínez, J. Jiménez, S. Ponce-Alcántara and V. Parra, Phys. Status Solidi (c) 8, 1330–1333 (2011).

[11] J. Chen, B. Chen, W. Lee, M. Fukuzawa, M. Yamada and T. Sekiguchi, Solid State Phenomena 156–158, 19–26 (2010).

This is a pre-print of an article published in Journal of Electronic Materials, 2018, Volume 47, Issue 9, pp 5077–5082.
The final authenticated version is available online at: https://doi.org/10.1007/s11664-018-6381-8

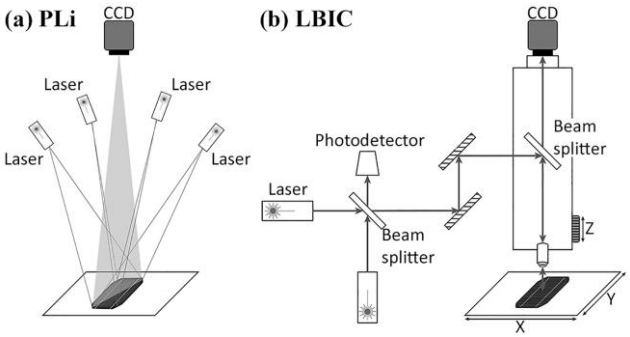

Fig. 1. (a) Scheme of the PLi system. (b) Scheme of the LBIC system.

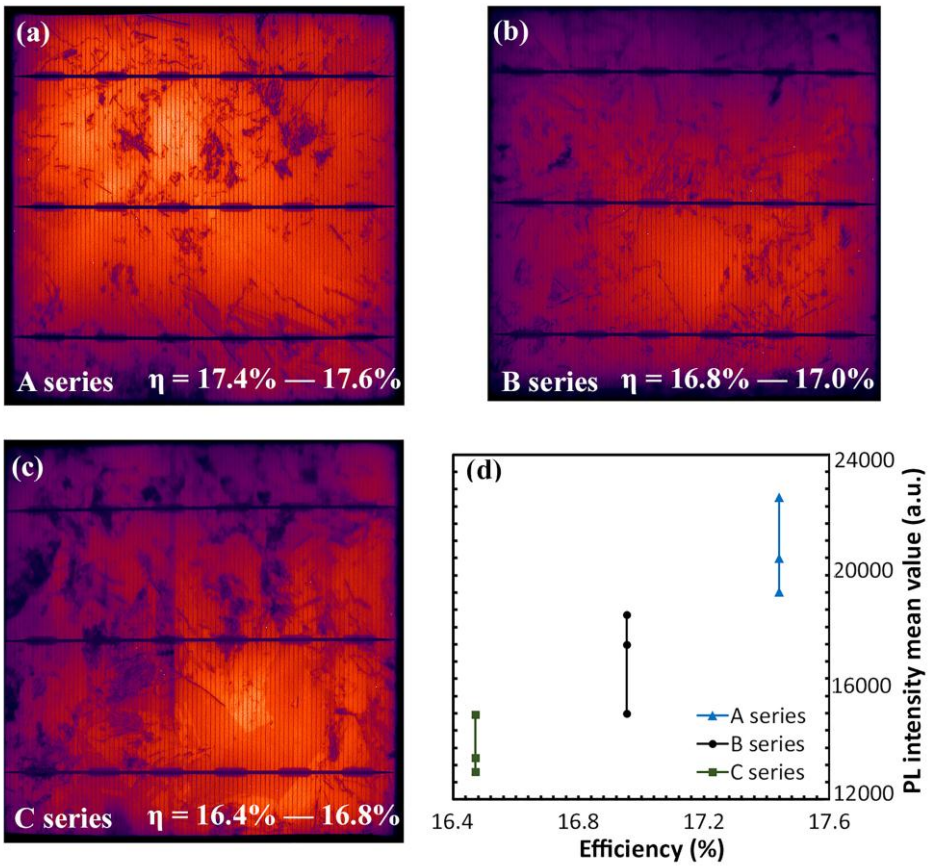

Fig. 2. (a—c) PL images of three solar cells of A, B and C series. (d) The PL intensity signal obtained for each series increases with the efficiency.

This is a pre-print of an article published in Journal of Electronic Materials, 2018, Volume 47, Issue 9, pp 5077–5082.
The final authenticated version is available online at: https://doi.org/10.1007/s11664-018-6381-8

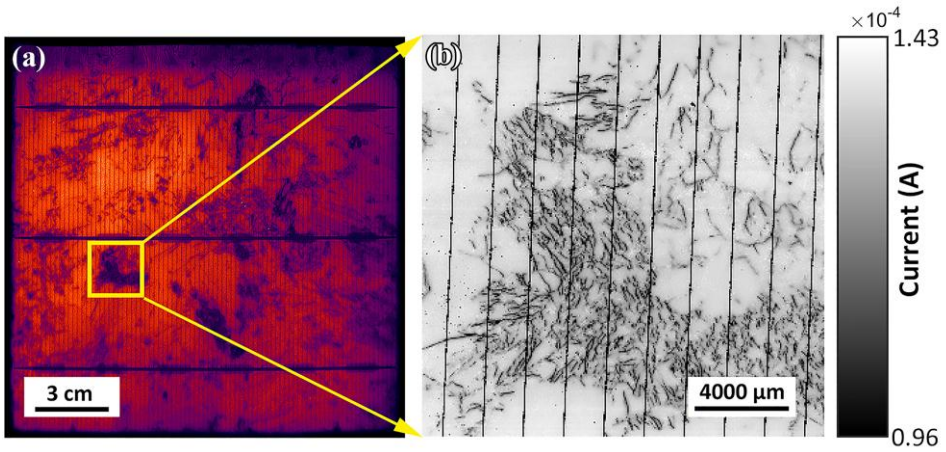

Fig. 3. (a) PL image of a C-series solar cell. (b) Corresponding LBIC map of the selected area in the PL image (18000x18000 µm^2, 20x objective, step size 60 µm).

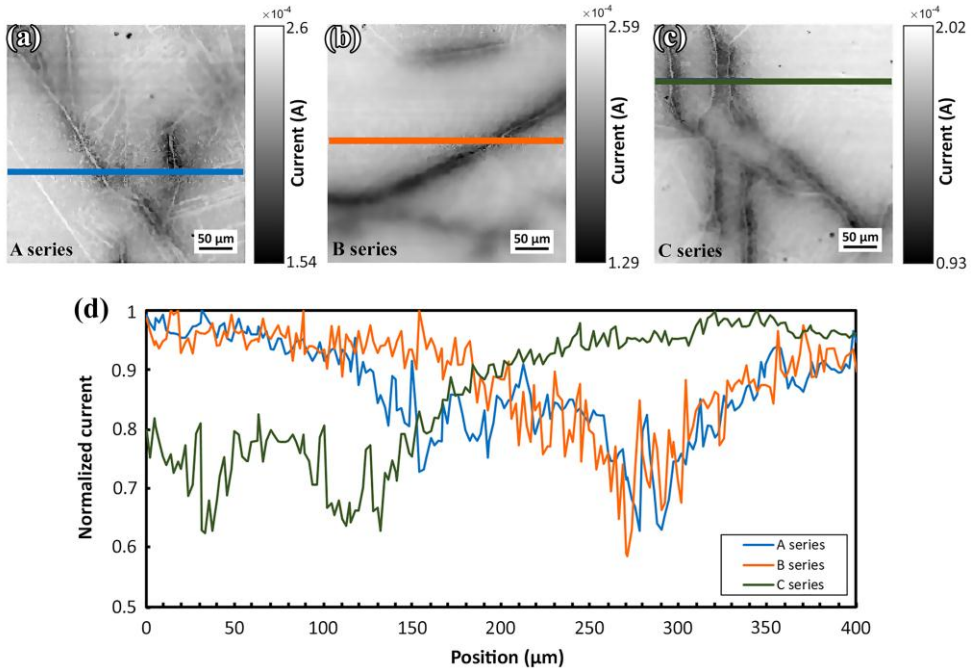

Fig. 4. (a—c) LBIC maps of defective areas in three solar cells of A, B and C series (400x400 µm^2, 100x objective, step size 2 µm). (d) Normalized photocurrent profiles across the lines marked in Fig. 4a—c.

This is a pre-print of an article published in Journal of Electronic Materials, 2018, Volume 47, Issue 9, pp 5077–5082.
The final authenticated version is available online at: https://doi.org/10.1007/s11664-018-6381-8

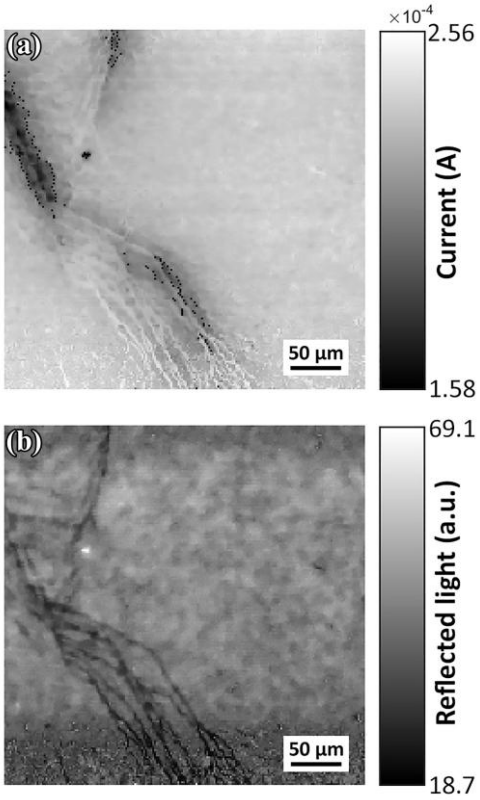

Fig. 5. (a) LBIC map of a C-series solar cell area presenting dark spots (400x400 µm^2, 100x objective, step size 2 µm). (b) Corresponding reflected light map. Some of the low reflective regions have a high electrical activity in the LBIC map, while others do not.